ChemPubSoc Europe

DOI: 10.1002/cbic.201800531

CHEMBIOCHEM Full Papers

Fluorescent Biosensor for Detection of the R248Q Aggregation-Prone Mutant of p53

Morgan Pellerano,[a] Delphine Naud-Martin,[b] Florence Mahuteau-Betzer,[b] Marie Morille,[c] and May C. Morris*[a]

The p53 tumour suppressor and guardian of the genome undergoes missense mutations that lead to functional inactivation in 50% of human cancers. These mutations occur mostly in the DNA-binding domain of the protein, and several of these result in conformational changes that lead to amyloid-like protein aggregation. Herein, we describe a fluorescent biosensor that reports on the R248Q mutant of p53 in vitro and in living cells, engineered through conjugation of an environmentally sensitive probe onto a peptide derived from the primary aggregation segment of p53. This biosensor was characterised both in vitro and by means of fluorescence microscopy following facilitated delivery into cultured cells. It is shown that this biosensor preferentially reports on the p53 R248Q mutant in the PC9 lung cancer cell line compared with other lung cancer cell lines harbouring either wild-type or no p53.

Introduction

The p53 protein was first identified in 1979 as a cellular protein physically associated with the simian virus SV40 large tumour antigen.[1–3] The subsequent finding that it was abundantly expressed in many tumours, compared with normal tissue, suggested that p53 might be a cellular oncogene.[3–5] Further studies revealed that p53 was a transcription factor induced by stress that played an important role in regulating expression of genes required for DNA repair to preserve DNA integrity, resulting in cell cycle arrest, apoptosis or senescence.[6–9] In unstressed cells, p53 levels are very low, but are rapidly induced and stabilised in response to various intra- and extracellular stresses, including DNA damage, hypoxia, oxidant metabolism, aging and oncogenic signalling, thereby promoting transcription of a wide variety of genes that modulate cellular functions (such as G1 arrest through induction of p21 or G2 arrest through induction of 14-3-3s, Gadd45 and p21), and consequently, playing a key role in maintaining genomic integrity and preventing tumour formation.[10–12] Today, p53 is recognised as one of the most functionally important proteins for cell cycle and transcriptional regulation and a major tumour suppressor.

p53 is a nuclear protein that tetramerises to bind DNA and regulate gene transactivation, and its transcriptional activity is critical for its tumour-suppressive functions because p53 mutation in human cancers abrogates its transcriptional activity.[13] Unfortunately, it is also the most frequently mutated protein in human cancers, with mutations or alternative splicing that invalidate its normal function occurring in approximately 50% of tumours.[8,9,14] Although most tumour-suppressor genes are deleted or truncated in human cancers, the TP53 gene frequently undergoes missense mutations, resulting in single amino acid substitutions, which cause loss of wild-type (WT) function, but may also exert a dominant negative effect through binding and inhibition of WT p53.[15] Moreover, several mutations result in gain of function, which endows p53 mutants with activities that contribute to hyperproliferation; increased tumourigenicity; anchorage-independent cell growth, metastasis and invasiveness; decreased sensitivity to chemotherapeutic drugs; disruption of the spindle checkpoint; activated topoisomerase I activity and induction of gene amplification.[5,15–17] For instance, the R175H gain-of-function mutation promotes activation of the multidrug resistance gene MDR1.[18] Gain of function R248Q and R273C mutants induce HER2 over-expression in cancer cells.[19] Moreover, p53 R248Q, but not R248W, has been shown to enhance in vitro invasiveness of human lung cancer NCI-H1299 cells.[20]

The WT p53 protein comprises an acidic and unstructured N-terminal domain that bears two transcriptional activation domains, TAD1 and TAD2, and a proline-rich domain (residues 1–100), a core DNA-binding domain (DBD; residues 102–292), a C-terminal region that contains a nuclear localisation signalling domain, an oligomerisation domain and a negative regulation

[a] M. Pellerano, Dr. M. C. Morris
Institut des Biomolécules Max Mousseron-IBMM-UMR 5247
Université de Montpellier, Faculté de Pharmacie
15, Av. Charles Flahault, 34093 Montpellier (France)
E-mail: may.morris@umontpellier.fr

[b] D. Naud-Martin, Dr. F. Mahuteau-Betzer
Institut Curie, PSL Research University
CNRS, INSERM, UMR9187-U1196
91405 Orsay (France)

[c] Dr. M. Morille
Institut Charles Gerhardt-UMR 5253 CNRS-UM-ENSCM
Université de Montpellier, Faculté de Pharmacie
15, Av. Charles Flahault, 34093 Montpellier (France)

Supporting information and the ORCID identification numbers for the authors of this article can be found under https://doi.org/10.1002/cbic.201800531.

This article is part of a Special Issue on Biosensing and Bioimaging.

domain (residues 293–393.[16,21–24] Beyond its ability to interact with gene transactivation sequences, the structural flexibility of p53 endows it with functional plasticity, which enables it to interact with protein partners involved in biological functions beyond transcription.[22,24,25] About 80% of the single-point missense mutations are located within the DBD, and about a third of these occur at six mutational hotspots: R175, G245, R248, R249, R273 and R282.[26–30] p53 mutants are commonly distinguished as "contact" and "structural" or "conformational" mutants, the former, including R273H or R248W, directly disrupting sequence-specific interactions between p53 and DNA, the latter, exemplified by R175H, G245S and R282W, inducing conformational changes that affect the thermodynamic stability of the protein, and consequently, the structural integrity of protein/DNA and protein/protein interaction interfaces.[21,22]

Both the N-terminal and core domains of p53 have been shown to form β-sheet-rich fibrillar aggregates in either mild denaturing or low-pH conditions.[31,32] Recent studies have suggested that the formation of p53 aggregates is associated with loss-of-function, dominant-negative and gain-of-function mutations and can be explained by a prion-like behaviour of mutant proteins.[33] Mutant p53 was shown to co-localise with amyloid-like protein aggregates in cancer biopsies.[34] Recent studies have shown that several structural mutants, in particular, R248Q, promote exposure of a domain that is naturally buried in WT p53 (251–257), leading to formation of amyloid-type aggregates of dysfunctional p53 in the cytoplasm.[35,36] Segment 251–257 has been reported as necessary and sufficient to drive p53 aggregation in vitro and in cell lines, although secondary structure prediction studies of the aggregation propensity of the p53 DBD reveal that several other regions are also prone to aggregation.[35–38] The R248Q mutant exhibits a particularly high tendency to partially unfold and has been inferred to display an increased aggregation propensity.[40] Moreover, NMR spectroscopy studies reveal that it induces conformational changes in the DBD far from the mutation site and beyond the site of interaction with DNA, associated with an aggressive gain of function, which induces early onset of cancer in Li–Fraumeni patients.[40,41] Finally, aggregated mutant p53 induces co-aggregation of WT p53 and its paralogs p63 and p73.[35]

Misfolded, aggregated p53 mutants constitute attractive targets for therapeutics that can restore WT structure and function. In this respect, a recent study by Soragni et al. demonstrated that a peptide derived from the aggregation domain could reverse mutant p53 aggregation and restore its nuclear localisation and function as a transcription factor in vivo.[36] Nevertheless, there are currently no tools that report on the conformational status of p53. To address this challenge, we have developed and characterised a fluorescent peptide biosensor that recognises the R248Q aggregation-prone mutant of p53. The biosensor was engineered through conjugation of an environmentally sensitive probe onto a peptide derived from the primary aggregation segment of p53 and characterised both in vitro and by means of fluorescence microscopy following facilitated delivery into cultured cells. This fluorescent peptide biosensor preferentially reports on the p53 mutant R248Q over that of WT p53 both in cell extracts and in cultured lung cancer cells.

Results and Discussion

Design and in vitro characterisation of a fluorescent peptide biosensor for detection of the R248Q mutant of p53

To probe mutants of p53, which have a tendency to aggregate, we took advantage of the aggregation-nucleating sequence (residues 251–257: ILTIITL) reported by Xu et al. within the DBD of p53, which induces aggregation of p53 mutants due to conformational changes promoting its exposure.[35] Because this motif self-aggregated if exposed, we hypothesised it constituted a good target for detection of the aggregation-prone mutant, and could also be used to engineer a biosensor for detection of R248Q. To this aim, we designed a 27 aa peptide derived from the aggregation sequence that spanned residues 248 to 274 (encompassing beta sheets S9 and S10) and in which we introduced a cysteine to replace isoleucine at position 254 (p254C peptide), to enable site-specific, thiol-mediated conjugation of a fluorescent probe (Scheme 1).

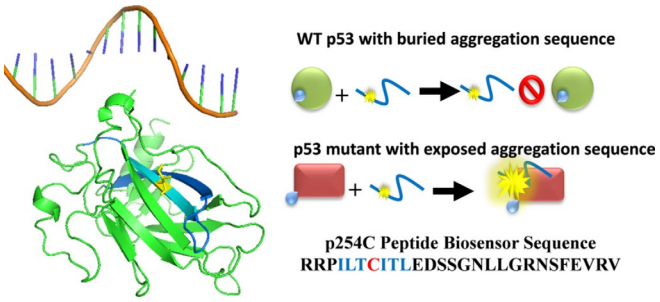

Scheme 1. The p254C peptide biosensor was derived from the S9–S10 β-sheets (residues 248–274, cyan) within the core DBD of p53 (green), harbouring the aggregation-nucleating sequence ILTIITL (251–257, cyan). I254 was replaced by a cysteine (yellow stick) for conjugation of an environmentally sensitive probe to generate a biosensor that preferentially recognises aggregation-prone mutants, in which this domain is exposed. PDB ID: 1TUP.

We first verified whether the p254C peptide could recognise the native peptide sequence derived from the p53 aggregation site, which is normally buried in WT p53, but exposed in aggregation-prone mutants, such as R248Q. To this aim, p254C was labelled with fluorescein isothiocyanate (FITC) and titrated with a peptide spanning beta sheets S9 and S10 and bearing an isoleucine at position 254 (p254I). This led to significant fluorescence enhancement, and curve fitting allowed us to determine a dissociation constant value of 913 nM ± 242 between these peptides, whereas titration of p254C-FITC with an irrelevant control (Ctrl) peptide,[42] or conversely titration of FITC-labelled Ctrl peptide with the p254I peptide, exhibited significantly lower changes in fluorescence emission (Figure 1 A).

We further asked whether the biosensor would potentially discriminate between WT p53 and the R248Q mutant. Experiments performed with GST-tagged recombinant proteins revealed preferential recognition of the R248Q mutant by

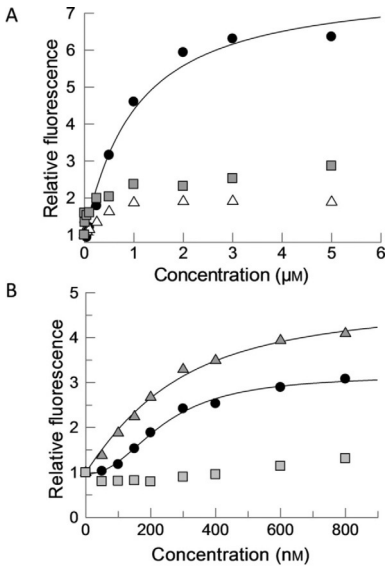

Figure 1. p254C-FITC binds the aggregation-nucleating sequence of p53. A) Fluorescence emission of 200 nM p254C-FITC following titration with the p254I peptide (●) or an irrelevant Ctrl peptide (■), or fluorescence emission of 200 nM irrelevant peptide labelled with FITC following titration with the p254I peptide (△). B) Fluorescence emission of 200 nM p254C-FITC following titration with recombinant glutathione S-transferase (GST)-tagged p53 (●), GST-tagged R248Q mutant (▲) or GST (■).

p254C-FITC, with a dissociation constant value of 240 nM ± 70, whereas GST WT p53 binding was much poorer, in the micromolar affinity, with a dissociation constant value of 252 μM ± 404 (Figure 1B and Table S1 in the Supporting Information), which was reminiscent of thioflavin T titration experiments previously reported by Bom et al., who showed that the R248Q mutant had a greater propensity to form amyloid-like aggregates under physiological conditions than that of WT p53 and could also seed aggregation of WT p53.[38]

To further explore the ability of the p254C peptide to probe the aggregation-nucleating sequence of p53, we asked whether it could report on its induced exposure if recombinant p53 was subject to thermo-denaturation. To this aim, we first asked whether other fluorescent probes than FITC might enable a greater response to R248Q, relative to WT p53 (Figure 2A). Results revealed TP2Rho, a highly sensitive water-soluble solvatochromic vinyltriphenylamine dye, which we previously used to probe peptide and protein interactions in vitro,[43,44] as the best candidate. We therefore prepared the p254C-TP2Rho conjugate (Scheme 2), for incubation with recombinant GST-tagged p53 expressed in *Escherichia coli*, purified by means of fast protein liquid chromatography (FPLC) and subjected to thermo-denaturation at different temperatures for 15 min. The fluorescence emission of p254C-TP2Rho was significantly enhanced following incubation of recombinant p53 at 60 and 95 °C; thus indicating greater recognition of the p254I motif, exposure of which was induced by thermo-denaturation (Figure 2B). In contrast, incubation of samples with thioflavin following thermal treatment revealed little if any aggregation under the conditions and concentrations used in our assay. These findings indicate that the p254C biosensor reports on heat-induced unfolding and exposure of the aggregation sequence, whereas thioflavin only responds to p53 aggregation. In contrast, the

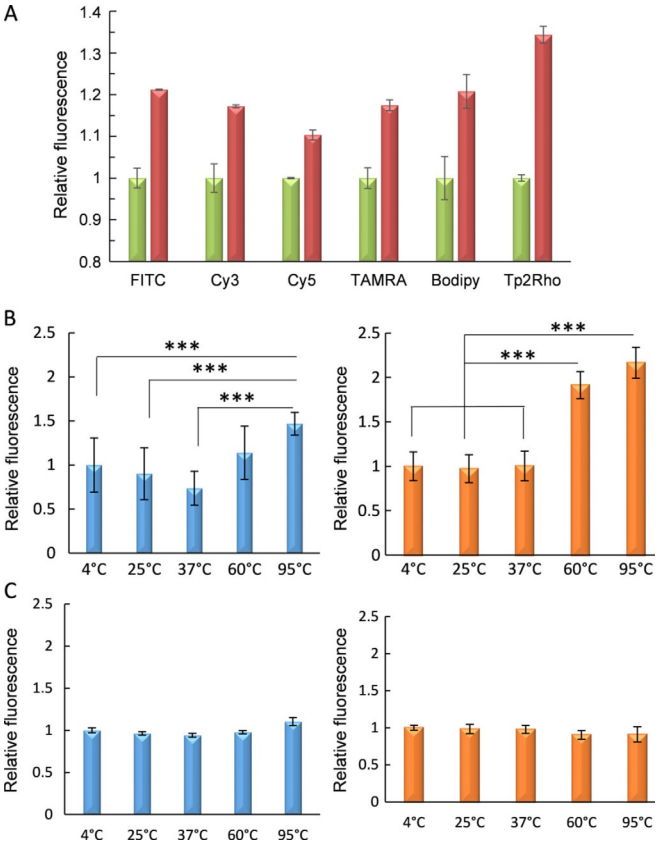

Figure 2. The p254C-TP2Rho biosensor responds preferentially to thermo-denatured p53. A) Relative fluorescence enhancement of the p254C-TP2Rho biosensor to WT (green) and R248Q (red) p53. B) Relative fluorescence enhancement of 25 μM thioflavin (blue) or 200 nM TP2Rho-labelled p254C (orange) following incubation with 1 μM recombinant GST-tagged p53 pre-incubated for 15 min at 4, 25, 37, 60 or 95 °C ($n=7$; student test: $^{***}p \leq 0.001$). C) Relative fluorescence enhancement of 25 μM thioflavin (blue) or 200 nM TP2Rho-labelled p254C (orange) following incubation with 1 μM recombinant Tau pre-incubated for 15 min at 4, 25, 37, 60 or 95 °C ($n=4$; student test reveals no statistically significant differences between values).

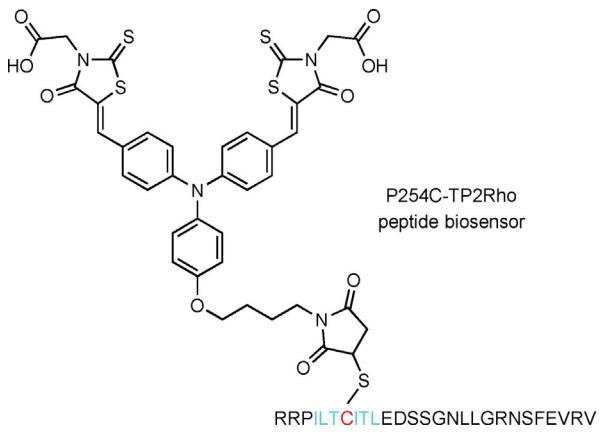

Scheme 2. The p254C-TP2Rho peptide biosensor derived from residues 248–274 of p53, which harbours the aggregation-nucleating sequence ILTIITL (251–257), in which I254 has been replaced by a cysteine for conjugation of the TP2Rho fluorophore.

FITC-labelled p254C biosensor did not respond to p53 denaturation (Figure S2A). Moreover, incubation of the thermostable microtubule-associated protein Tau had no effect on either the p254C biosensor or thioflavin fluorescence following treatment at higher temperatures, in line with the well-known lack of Tau denaturation (Figure 2C). Likewise, incubation of TP2Rho alone, or of the TP2Rho-labelled Ctrl peptide, with thermodenatured p53 did not promote any significant fluorescence enhancement; thus indicating that TP2Rho probe did not respond non-specifically (Figure S2B).

To gain further insight into the behaviour of TP2Rho-p254C, we asked whether it might potentially self-aggregate. However, this appears unlikely because increasing concentrations of the p254C-TP2Rho biosensor exhibit a significant and linear increase in both absorbance and fluorescence emission, whereas the response of TP2Rho alone is less linear (Figure S2C and D). p254C-TP2Rho was further investigated by means of nanoparticle tracking analysis (NTA) relative to the p254C peptide, TP2Rho alone, Ctrl peptide alone and TP2Rho-labelled Ctrl peptide (Figure S2E). Results revealed a very small proportion of particulate entities in solution for all of these peptides, whether labelled or not, and more so for TP2Rho alone or for the labelled Ctrl peptide, but not representative of aggregates, compared with a standard reference (Aβ peptide[45]). Finally, we determined the quantum yield of TP2Rho, p254C-TP2Rho and p254C-TP2Rho in the presence of the R248Q mutant, in phosphate-buffered saline (PBS) and relative to rhodamine (Figure S3). Calculated values reveal that the quantum yield of TP2Rho conjugated onto p254C undergoes a significant increase relative to that of TP2Rho in PBS: ϕ TP2Rho $\leq$0.005 and ϕ p254C-TP2Rho: 0.07. The quantum yield increases further if p254C-TP2Rho is incubated with the R248Q mutant: ϕ p254C-Tp2Rho/ R248Q: 0.20.

The p254C peptide biosensor discriminates between the R248Q mutant and WT p53 in lung cancer cell extracts

To characterise the p254C biosensor in a more physiological environment, we chose to use cell extracts from the PC9 lung cancer cell line, which expressed the R248Q mutant. To assess the abundance of this mutant in PC9 cell extracts, we performed western blotting of recombinant GST-p53 R248Q to establish a calibration curve and compared the signal corresponding to R248Q in 20 μg PC9, thereby determining an average concentration of 170 nM p53 R248Q (Figure S4A).

To choose the most suitable probe for the p254C biosensor, we conjugated the p254C peptide to several fluorescent probes and assayed their response following incubation with 40 μg PC9 cell extracts (Figure 3A). The TP2Rho probe yielded by far the greatest response, with a 12-fold fluorescence enhancement of basal biosensor fluorescence emission in the absence of cell extracts, and was therefore selected for further experiments. Moreover, we noticed that the fluorescence emission of TP2Rho-labelled biosensor was somewhat greater upon excitation at λ=392 nm and emission acquired between λ=510 and 570 nm, compared with excitation at λ=510 nm followed by fluorescence emission at λ=614 nm (Figure S5).

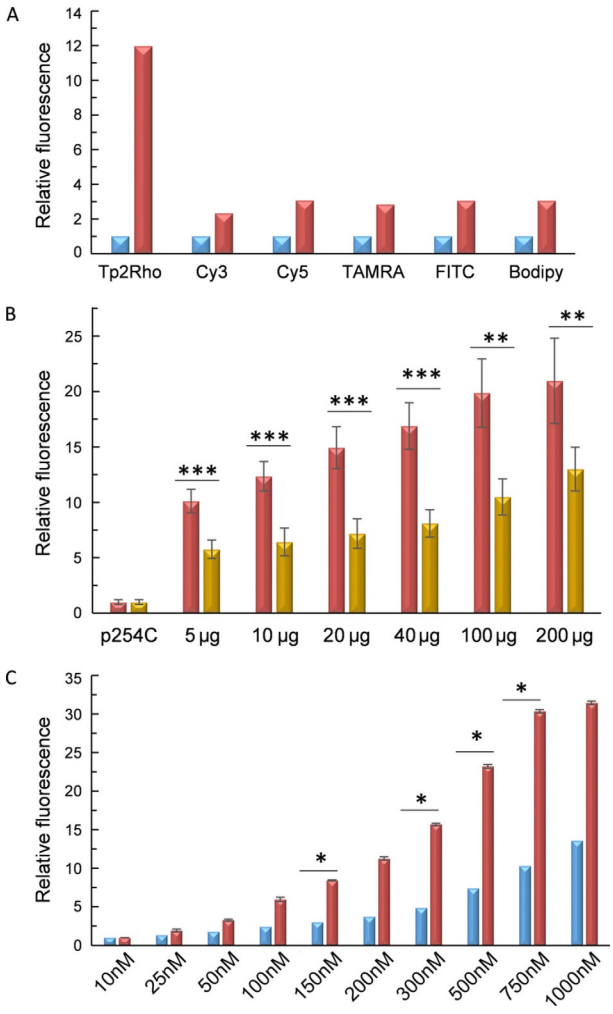

Figure 3. Characterisation and optimisation of the p53 response to R248Q in PC9 lung cancer cell extracts. A) Maximal fluorescence enhancement of 200 nM p53 biosensor labelled with TP2Rho (λ_{ex}=392 nm; λ_{em}=510 nm), Cy3 (λ_{ex}=530 nm; λ_{em}=580 nm), Cy5 (λ_{ex}=610 nm; λ_{em}=675 nm), tetramethylrhodamine (TAMRA; λ_{ex}=535 nm; λ_{em}=585 nm) and FITC (λ_{ex}=483 nm; λ_{em}=530 nm), incubated with (red) or without (blue) 40 μg PC9 cell extracts (p53 R248Q). B) Dose-dependent response of 200 nM TP2Rho–biosensor (λ_{ex}=392 nm; λ_{em}=510 nm) to increasing amounts of PC9 (red; p53 R248Q) cell extracts from 5 to 200 μg (n=5; student test: **$p \leq 0.01$; ***$p \leq 0.001$); BSA (orange) was used as a negative control. C) Dose-dependent response of 40 μg PC9 (red) extract to increasing concentrations of TP2Rho–biosensor (λ_{ex}=392 nm; λ_{em}=510 nm) from 50 nM to 1 μM (n=3; student test: *$p \leq 0.05$) compared to the biosensor alone without any cell extracts (blue).

These conditions were therefore retained for all further experiments performed with cell extracts. To determine the optimal concentrations of cell extracts, on the one hand, and the most suitable concentration of TP2Rho-labelled biosensor on the other, to achieve the most significant and sensitive response, we performed dose-dependent experiments with 5 to 200 μg cell extracts and 50 nM to 1 μM biosensor (Figure 3B and C). With 200 nM p254C-TP2Rho biosensor, we observed a dose-dependent increase in fluorescence enhancement of TP2Rho, in response to increasing concentrations of PC9 cell extracts, in line with an expected increase in biosensor response to increased p53 levels, with a saturating response at 100–200 μg

extract. In comparison, bovine serum albumin (BSA) induced much less fluorescence enhancement, with an optimum for 20–40 μg extracts, which become more important at higher concentrations of BSA, indicating loss of specific response. Conversely, we observed a dose-dependent response of increasing biosensor concentrations to 40 μg PC9 extracts, with a plateau at around 750–1000 nM biosensor. Taken together, these results indicate that the p254C biosensor can detect nanomolar concentrations of p53 mutant in cell extracts, and that the dynamic range of response varies up to 20-fold fluorescence enhancement.

Based on these results, we selected intermediate conditions (200 nM biosensor–TP2Rho and 40 μg protein extracts) for further experiments, to limit the non-specific response of irrelevant proteins, such as BSA.

To further validate the utility of this biosensor to detect the R248Q mutant, we next asked whether it could report on differences between three lung cancer cell lines: A549 (p53WT) PC9 (p53 R248Q) or H1299 (p53−/−). Normalised cell extracts prepared from A549, expressing p53 WT, PC9 expressing the mutant p53 R248Q and H1229 lacking p53 were incubated with 200 nM p254C-TP2Rho biosensor. These experiments revealed that the relative increase in p254C-TP2Rho fluorescence emission upon incubation with protein extracts containing p53 R248Q was 83% greater than that with extracts expressing WT p53 or lacking p53 (Figure 4A and Table S2).

To confirm these fluorescence-based experiments, we performed pull-down experiments by immobilising the p254C peptide on CNBr-Sepharose. Western blotting of the samples incubated with the biosensor-conjugated beads revealed that only the p53 R248Q mutant was expressed in PC9 cell extracts, but no WT p53 expressed in A549 cells was retained by the biosensor (Figure S4B).

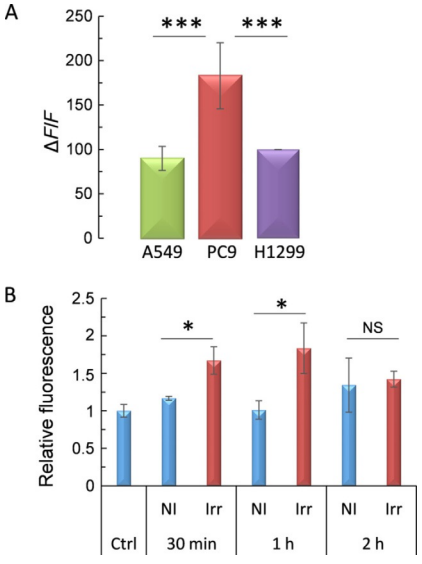

Figure 4. Quantification of the p53 biosensor response to WT p53 and R248Q mutant in different lung cancer cell extracts. A) Relative fluorescence emission of 200 nM TP2Rho–biosensor to 40 μg A549 (p53WT), PC9 (p53 R248Q) and H1299 (p53−/−) lung cancer cell extracts ($n=17$; student test: *** $p \leq 0.001$). B) Response of p254C-TP2Rho to induction of the p53 R248Q mutant in PC9 cells following UV irradiation (IRR; NI: no irradiation; $n=4$; student test: * $p \leq 0.05$).

Because p53 is induced by UV-B irradiation,[11] we asked whether the p254C biosensor was sufficiently sensitive to monitor differences in R248Q protein expression following irradiation of PC9 cells with UV-B (300 mJ cm^{-2}), which were then returned to the incubator to allow for protein expression, and harvested after 30 min; 1 h or 2 h to assess the relative levels of p53 mutant expression with the p254C-TP2Rho biosensor. This experiment revealed that R248Q expression was induced after 30 min and maximal after 1 h (Figure 4B). In contrast, the biosensor did not report on any significant difference in the A549 cell line, which expressed WT p53; thus again underscoring its preferential response to the R248Q mutant (Figure S6).

The p53 biosensor reports on the R248Q mutant in living cells

Having established the optimal working conditions and limitations of the biosensor in vitro, we asked whether we could apply it to report on the R248Q mutant in living cells by fluorescence imaging. To this aim, we first introduced the biosensor into cultured cells thanks to the amphipathic cell-penetrating peptide Pep1 (Figure 5).[46] Control experiments showed that the TP2Rho-labelled p254C peptide could not enter cells alone. In contrast, complexation of p254C-TP2Rho with Pep1 at a 1:40 molar ratio enabled efficient and homogeneous delivery into PC9 cells (Figure S7 and S8A).

We therefore introduced p254C-TP2Rho into PC9 and A549 cells and acquired their relative fluorescence emission, which we quantified relative to the nuclear DNA staining signal with Hoechst dye (Figure 6 and Table S3). These experiments revealed a significantly greater fluorescence ratio (twofold) in the PC9 cell line that expressed the R248Q mutant compared with that in the A549 cell line (Table S3); thus indicating that the p254C biosensor is a useful tool to monitor the expression of the R248Q mutant in living cells.

Finally, we asked whether biosensor internalisation might induce any toxicity. Crystal violet assays revealed that neither p254C-TP2Rho alone, nor complexed with Pep1, led to any significant inhibition of cell viability (Figure S8B).

Conclusion

Several therapeutic strategies have been proposed to target mutant p53 in cancer, including gene therapy, restoring WT p53 function thanks to small molecules, promoting mutant p53 degradation and/or targeting mutant p53 regulated pathways.[8,39] The more recent discovery of the prion-like properties of p53 aggregates has provided further insight into the molecular basis of p53 regulation and opened up new avenues to explore therapeutic strategies. Indeed, targeting the amyloid-like aggregation of p53 mutants in ovarian cancer has recently been demonstrated to constitute an effective therapeutic strategy for rescuing p53 tumour suppression.[36,39]

50% of human cancers harbour p53 mutations, most of which are missense mutations within the DBD, and several of

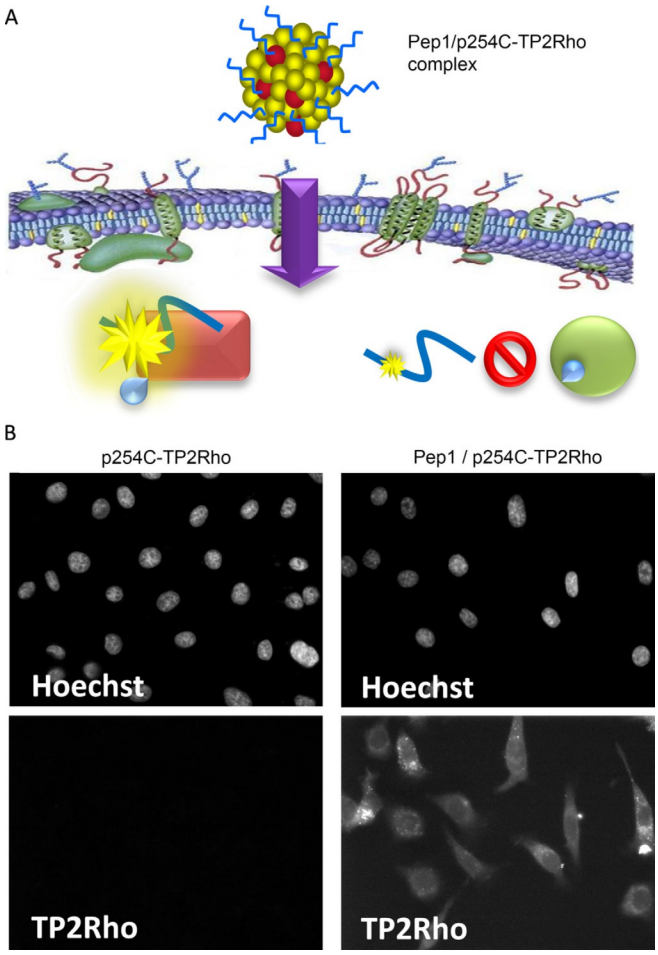

Figure 5. Internalisation of the p254C-TP2Rho biosensor in living cells. A) Schematic representation of complexation and facilitated delivery of Pep1/ p254C-TP2Rho peptide into living cells. B) Fluorescence micrographs illustrating internalisation of p254C-TP2Rho in PC9 cells following overlay of the Pep1/biosensor complexes, but not of the biosensor alone. Nuclear staining with Hoechst dye is shown in the upper panels; TP2Rho fluorescence is shown in the lower panels (Cy3 filter of the microscope).

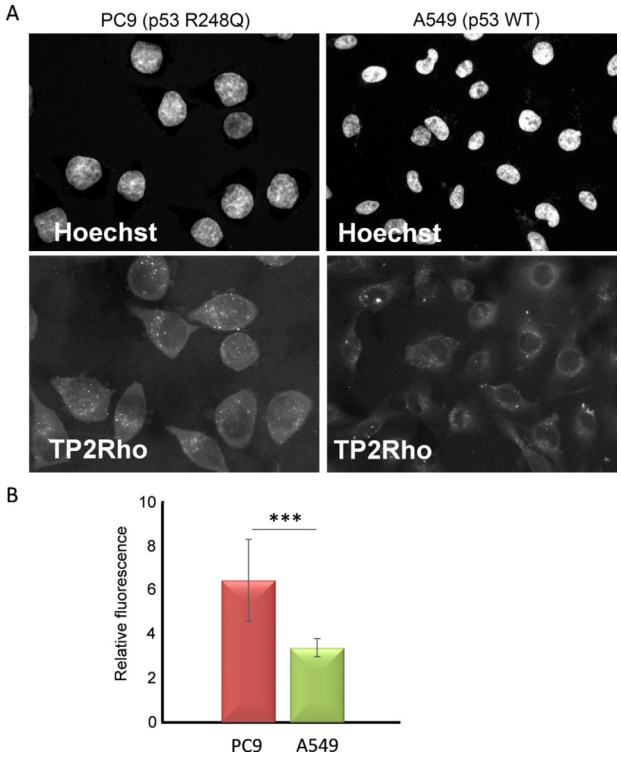

Figure 6. Response of the p254C-TP2Rho biosensor to the WT and R248Q mutant in lung cancer cells. A) Micrographs of A549 and PC9 cells into which the p254C-TP2Rho biosensor was delivered following complexation with Pep1. Nuclear staining with Hoechst dye is shown in the upper panels; TP2Rho fluorescence is shown in the lower panels (Cy3 filter of the microscope). B) Ratiometric quantification analysis of $n = 9$ different regions of interest (ROIs) from acquisitions of TP2Rho and Hoechst dye signals in A549 and PC9 cell lines ($n = 9$: student test: $^{***}p \leq 0.001$).

these mutants have been shown to be prone to aggregation, due to structural destabilisation, although the actual fraction of aggregated p53 mutant remains unknown. Current diagnostic approaches based on genetic sequencing allow the identification of specific mutations in p53, but they do not inform on its conformational status. Tools enabling probing and reporting on differential structural organisations, such as misfolding and exposure of aggregation-nucleating epitopes, would be of major benefit to complete molecular profiling studies.

In this study, we reported on the design and characterisation of a fluorescent peptide biosensor derived from the main aggregation-nucleating motif of p53, for detection of the R248Q mutant. This biosensor was engineered through conjugation of a highly sensitive solvatochromic dye, TP2Rho, that we previously implemented to monitor protein–protein and protein–peptide interactions in vitro.[44] We have shown that this biosensor interacts with the self-aggregation motif of p53 itself in vitro and that it preferentially interacts with recombinant R248Q mutant over WT p53. This biosensor further reports on exposure of the self-aggregation domain of p53 upon thermodenaturation, in a sensitive fashion, prior to detection of protein aggregates by thioflavin. We have also shown that this biosensor can detect nanomolar concentrations and discriminate between R248Q and WT p53 in lung cancer cell extracts in both fluorescence-based and pull-down experiments. The relative increase in p254C-TP2Rho fluorescence emission upon incubation with protein extracts containing p53 R248Q was 83% greater than that with extracts expressing p53WT or lacking of p53. Finally, we have shown that delivery of this biosensor into living cells enables quantification of relative differences between cell lines expressing R248Q and WT p53 by means of fluorescence imaging.

Because the R248Q mutant has been identified as a gain-of-function aggressive mutant that enhances in vitro invasiveness of human lung cancer cells,[20] the biosensor we have developed could constitute a useful tool to quantify this conformationally destabilised mutant in lung cancer biopsies and guide towards appropriate treatments. The most straightforward application of this new tool is its implementation for ex vivo diagnostics through measurement of fluorescence emission upon incubation with protein samples. Moreover, the peptide nature of this biosensor enables simultaneous acquisition and comparison of several samples in a plate reader. Beyond the diagnostic potential of this biosensor, it has an clear and natu-

ral purpose for drug discovery because it could enable screening of compounds that could reverse mutant aggregation-prone conformation to restore WT function. A second application of interest would involve intracellular internalisation of the biosensor and fluorescence imaging to identify the presence of misfolded p53 and potentially investigate the heterogeneity of cells. Because it cannot be excluded that the efficiency of internalisation of the cell-penetrating peptide/biosensor complexes may differ between cell lines, it would be wise to normalise biosensor response to its intracellular levels if different cell lines are being studied. This tool could also allow the appearance of misfolded p53 mutants to be followed over time, and upon exposure to mutation-inducing environments or reagents that might affect p53 folding. Ultimately, the biosensor could serve to develop companion assays to monitor the therapeutic efficacy of drugs capable of reversing p53 aggregation.

Experimental Section

Design, synthesis and labelling of the peptide biosensor: The p53 peptide biosensor was derived from the sequence of the S9-S10 β sheets, harbouring the aggregation domain of p53 (residues 248–274), in which Ile254 was replaced by a cysteine to enable site-specific labelling with fluorescent probes. RRPILTCITLEDSSGNLLGRNSFEVRV p254C peptide and the native p254I peptide RRPILTIITLEDSSGNLLGRNSFEVRV were synthesised by using the fluorenylmethyloxycarbonyl (Fmoc) strategy with the liberty blue robot from CEM. Peptides were purified by HPLC and the purity was analysed by LCMS (see the Supporting Information). p254C was then labelled on the single cysteine residue with FITC, TP2Rho, or other maleimide dye derivatives, in the presence of a five- to tenfold excess of dye overnight, and then purified from free dye on NAP-5 columns (GE Healthcare). Ctrl peptide: VESSDTIDNVKSKIQDKEGC was synthesised by GLS Biochem.[42]

Protein expression and purification: Recombinant WT GST-p53 and GST-p53 R248Q mutant were expressed in *E. coli* (BL21 DEA3) following induction with 1 mM isopropyl β-D-1-thiogalactopyranoside (IPTG) for 3 h at 37 °C and purified by FPLC on a GSTrap HP 5 mL column (GE Healthcare) equilibrated in buffer A (50 mM phosphate, pH 7.4, 150 mM NaCl). GST-tagged proteins were eluted with buffer A containing glutathione (50 mM; Euromedex), and then further injected onto a desalting column (GE Healthcare) equilibrated in buffer A to eliminate free glutathione. Recombinant Tau was expressed in *E. coli* following induction with 1 mM IPTG for 3 h at 37 °C. The soluble-protein fraction was incubated for 15 min at 75 °C. After centrifugation, the supernatant was incubated with 60% ammonium sulfate overnight. After centrifugation, the pellet was resuspended in buffer B (50 mM TRIS, pH 7.4, 150 mM NaCl) and purified by FPLC on a HiLoad 16/600 Superdex 75 prep-grade column (GE Healthcare) equilibrated in buffer B.

Recombinant protein thermo-denaturation and fluorescence experiments: For thermo-denaturation experiments, 1 μM recombinant GST-p53 was incubated for 15 min at 4, 25, 37, 60 and 95 °C. Fluorescence titration assays were performed in 96-well plates thermostatted at 30 °C with a Clariostar spectrofluorimeter (BMG). Samples (200 μL) were prepared in potassium phosphate buffer (50 mM KH_2PO_4/K_2PO_4 pH 7.4, 150 mM NaCl, 200 nM). FITC-labelled peptides were excited at $\lambda = 483$ nm, and emission signals were acquired at $\lambda = 530$ nm. TP2Rho-labelled peptides were excited at $\lambda = 510$ nm and fluorescence emission was acquired at $\lambda = 614$ nm. Thioflavin fluorescence emission was monitored at $\lambda = 492$ nm following excitation at $\lambda = 450$ nm. Experiments were performed in triplicate, and error bars indicate standard deviations from averages.

Curve fitting and determination of dissociation constants for peptide/peptide and GST-R248Q p53/biosensor binding were performed with the GraFit software (Erithacus, Ltd., Horley, UK) by using quadratic Equation (1):

$$F = F_{max} + (F_{max} - F_{min}) \times \frac{K_d + L + p - \sqrt{(\sqrt{(K_d + L + p)^2 - 4p})}}{2p} \quad (1)$$

in which L is the concentration of ligand and p is the concentration of fluorescent peptide biosensor.

Curve fitting and determination of dissociation constants for GST-WT p53/ biosensor interactions was performed by using a cooperative fitting of Equation (2) (+ background):

$$y = \frac{[L]^n \times Cap}{(K_d + [L])^n} + background \quad (2)$$

In which L is the concentration of ligand, Cap is the capacity and n is the cooperativity.

Determination of quantum yield (ϕ): Fluorescence quantum yields of TP2Rho, p254C-TP2Rho or p254C-TP2Rho with p53 R248Q were calculated by using rhodamine R (in ethanol) as a standard ($\phi = 0.95$). Fluorescence emission spectra were recorded between $\lambda = 570$ and 670 nm following excitation at $\lambda = 560$ nm for the standard, and between $\lambda = 550$ and 720 nm following excitation at $\lambda = 510$ nm for samples. Absorbance was recorded at $\lambda = 560$ nm for the standard and at $\lambda = 510$ nm for the samples. Quantum yields were calculated according to Equation (3), in which ϕ_{ref} is the quantum yield of the reference; A_{sample} and A_{ref} are the areas under the emission spectra of the sample and reference, respectively; OD_{sample} and OD_{ref} are the absorbances of the sample and reference, respectively, measured at the excitation wavelength; and n_{sample} and n_{ref} are the refractive indices of the sample (PBS: 1.33) and reference (ethanol: 1.47), respectively.

$$\phi_{sample} = \phi_{ref} \frac{A_{sample}}{A_{ref}} \times \frac{OD_{ref}}{OD_{sample}} \times \left(\frac{n_{ref}}{n_{sample}}\right)^2 \quad (3)$$

NTA: NTA measurements were performed with a NanoSight NS 300 instrument (Malvern Panalytical, UK) equipped with a $\lambda =$ 405 nm laser and a temperature-controlled sample chamber. After a 5 min sonication step, peptide suspensions (200 nM peptide or probe) were injected into the chamber by using a syringe pump at 40 AU (arbitrary unit). The temperature was set at 25 °C and three videos of 60 s were recorded. Videos were then analysed by using the NanoSight NTA 3.2 software (the threshold was fixed at 5 for all measurements).

Cell culture, UV irradiation and cell-extract preparation: Cell culture media were purchased from Life Technology. Serum and antibiotics were purchased from Sigma. All cell lines were cultured in RPMI + Glutamax supplemented with 10% foetal calf serum (FCS), 100 units mL^{-1} penicillin (G sodium salt) and 100 μg mL^{-1} streptomycin at 37 °C in an atmosphere containing 5% CO_2. Lung cancer cell lines used in this study: A549: p53 WT; PC9: p53 R248Q mutant; H1299: p53 −/−. Cell extracts were prepared in PBS lysis

buffer containing PBS (Sigma), pH 7.4, 150 mM NaCl, 0.2% NP40, 1 mM ethylenediaminetetraacetic acid (EDTA), 2 mM phenylmethane sulfonyl fluoride (PMSF) and complete protease inhibitors (Roche), and normalised following spectrophotometric dosage at $\lambda = 280$ nm. Cells were irradiated with UV-B at 300 mJ cm^{-2} (Waldmann 800 K), then returned to the incubator and scraped after 30 min, 1 h or 2 h to prepare cell extracts. Fluorescence experiments with cell extracts were performed in 96-well plates thermostatted at 30 °C with a Clariostar spectrofluorimeter (BMG). Samples (200 μL) were prepared in potassium phosphate buffer (50 mM, pH 7.4, 150 mM NaCl). Tp2Rho-labelled peptides (200 nM) were excited at $\lambda = 392$ nm, and emission signals were acquired at $\lambda = 510$ nm.

Pull-down assays and western blotting: The p254C peptide was coupled onto CNBr Sepharose resin (10^{-3} M peptide per g resin; GE Healthcare) and incubated with 200 μg cell extracts from A549 (p53 WT), PC9 (p53 R248Q) or H1299 (p53−/−) for 1 h at 4 °C, washed twice in PBS, and the resin was boiled in Laemmli and loaded onto SDS-PAGE. Western blotting was performed following transfer of proteins onto polyvinylidene fluoride (PVDF) membrane, pre-blocked with 5% milk/TRIS-buffered saline (TBS), with the anti-p53 antibody DO-1 in TBS/Tween.

Cell culture, internalisation and microscopy: For introduction into living cells, p254C-TP2Rho was complexed with the cell-penetrating peptide Pep1[46] (1:40, molar ratio unless otherwise stated) and overlaid onto cultured cells grown to sub-confluency for 1 h at 37 °C, then for 16 h in the presence of RPMI + Glutamax complemented with 10% serum. Cells were then fixed with 4% paraformaldehyde in PBS for 10 min, washed with PBS and nuclei stained with Hoechst, washed with water and mounted on glass slides in Mowiol. Fluorescent cells were observed with a Zeiss microscope equipped with a CoolSnap camera and images were acquired by using MetaMorph software. Excitation band/dichroic/emission band filters for imaging fluorescent signals were as follows: Hoechst: $\lambda = 340–380/400/450–490$ nm; TP2Rho fluorescence was imaged by using Cy3 filters: $\lambda = 525–565/565/572–647$ nm. For quantification of biosensor fluorescence emission, images were analysed by using ImageJ software and average pixel intensity determined in ROIs corresponding to groups of three to four cells ($n = 9$). TP2Rho fluorescence was normalised to that of Hoechst dye in the ROIs.

Cell viability assays: PC9 cells were grown to sub-confluency for 24 h and overlaid with p254C-TP2Rho or p254C-TP2Rho/Pep1 complexes prepared as described above. After 24 h, cell proliferation was determined by means of crystal violet staining. Cells were washed with PBS, fixed with 3.7% formaldehyde for 10 min and then incubated with 0.1% crystal violet dye for 30 min. After rinsing, crystals were dissolved in 10% acetic acid and viability was determined by absorbance at $\lambda = 595$ nm with a microplate reader.

Statistics: Statistical significance was calculated through the student's test: $*p \leq 0.05$, $**p \leq 0.01$, $***p \leq 0.001$

Acknowledgements

This work was supported by the CNRS (Centre National de la Recherche Scientifique). We thank Dr. Pierre Roux, CRBM, Montpellier for critical advice. This study benefited from the facilities and expertise of the Montpellier RIO Imaging Facility (www.mri.cnrs.fr) at the Centre de Recherches en Biochimie Macromoléculaire, Montpellier, and of the SynBio3 Peptide Synthesis and Purification Facility supported by IBISA and ITMO Cancer of the Department of Amino Acids Peptides and Proteins (DAPP) at the Institut des Biomolécules Max Mousseron in Montpellier.

Conflict of Interest

The authors declare no conflict of interest.

Keywords: aggregation · biosensors · cancer · fluorescence · peptides

[1] D. P. Lane, L. V. Crawford, *Nature* **1979**, *278*, 261 – 263.
[2] C. Chang, D. T. Simmons, M. A. Martin, P. T. Mora, *J. Virol.* **1979**, *31*, 463 – 471.
[3] D. I. Linzer, A. J. Levine, *Cell* **1979**, *17*, 43 – 52.
[4] A. B. DeLeo, G. Jay, E. Appella, G. C. Dubois, L. W. Law, *Proc. Natl. Acad. Sci. USA* **1979**, *76*, 2420 – 2424.
[5] R. Brosh, V. Rotter, *Nat. Rev. Cancer* **2009**, *9*, 701 – 713.
[6] D. P. Lane, *Nature* **1992**, *358*, 15 – 16.
[7] K. Harms, S. Nozell, X. Chen, *Cell. Mol. Life Sci.* **2004**, *61*, 822 – 842.
[8] A. J. Levine, M. Oren, *Nat. Rev. Cancer* **2009**, *9*, 749.
[9] K. H. Vousden, D. P. Lane, *Nat. Rev. Mol. Cell Biol.* **2007**, *8*, 275 – 283.
[10] K. H. Vousden, *Biochim. Biophys. Acta Rev. Cancer* **2002**, *1602*, 47 – 59.
[11] G. Liu, X. Chen, *J. Cell. Biochem.* **2006**, *97*, 448 – 458.
[12] K. H. Vousden, C. Prives, *Cell* **2009**, *137*, 413 – 431.
[13] B. Vogelstein, K. W. Kinzler, *Cell* **1992**, *70*, 523 – 526.
[14] P. A. J. Muller, K. H. Vousden, *Nat. Cell Biol.* **2013**, *15*, 2 – 8.
[15] J. Liu, C. Zhang, Z. Feng, *Acta Biochim. Biophys. Sin.* **2014**, *46*, 170 – 179.
[16] W. A. Freed-Pastor, C. Prives, *Genes Dev.* **2012**, *26*, 1268 – 1286.
[17] S. Liu, J. K. Bolger, L. O. Kirkland, P. N. Premnath, C. McInnes, *ACS Chem. Biol.* **2010**, *5*, 1169 – 1182.
[18] K. V. Chin, K. Ueda, I. Pastan, M. M. Gottesman, *Science* **1992**, *255*, 459 – 462.
[19] A. A. Román-Rosales, E. García-Villa, L. A. Herrera, P. Gariglio, J. Díaz-Chávez, *BMC Cancer* **2018**, *18*, 709.
[20] K. Yoshikawa, J. Hamada, M. Tada, T. Kameyama, K. Nakagawa, Y. Suzuki, M. Ikawa, N. M. M. Hassan, Y. Kitagawa, T. Moriuchi, *Biomed. Res.* **2010**, *31*, 401 – 411.
[21] Y. Cho, S. Gorina, P. D. Jeffrey, N. P. Pavletich, *Science* **1994**, *265*, 346 – 355.
[22] A. C. Joerger, A. R. Fersht, *Annu. Rev. Biochem.* **2008**, *77*, 557 – 582.
[23] S. Surget, M. P. Khoury, J.-C. Bourdon, *OncoTargets Ther.* **2013**, *7*, 57 – 68.
[24] A. L. Okorokov, M. B. Sherman, C. Plisson, V. Grinkevich, K. Sigmundsson, G. Selivanova, J. Milner, E. V. Orlova, *EMBO J.* **2006**, *25*, 5191 – 5200.
[25] M. F. Lavin, N. Gueven, *Cell Death Differ.* **2006**, *13*, 941 – 950.
[26] P. Hainaut, T. Hernandez, A. Robinson, P. Rodriguez-Tome, T. Flores, M. Hollstein, C. C. Harris, R. Montesano, *Nucleic Acids Res.* **1998**, *26*, 205 – 213.
[27] S. A. Forbes, N. Bindal, S. Bamford, C. Cole, C. Y. Kok, D. Beare, M. Jia, R. Shepherd, K. Leung, A. Menzies, J. W. Teague, P. J. Campbell, M. R. Stratton, P. A. Futreal, *Nucleic Acids Res.* **2011**, *39*, D945.
[28] D. Walerych, M. Napoli, L. Collavin, G. Del Sal, *Carcinogenesis* **2012**, *33*, 2007 – 2017.
[29] C. Kandoth, M. D. McLellan, F. Vandin, K. Ye, B. Niu, C. Lu, M. Xie, Q. Zhang, J. F. McMichael, M. A. Wyczalkowski, M. D. M. Leiserson, C. A. Miller, J. S. Welch, M. J. Walter, M. C. Wendl, T. J. Ley, R. K. Wilson, B. J. Raphael, L. Ding, *Nature* **2013**, *502*, 333.
[30] M. Olivier, S. P. Hussain, C. Caron de Fromentel, P. Hainaut, C. C. Harris, *IARC Sci. Publ.* **2004**, 247 – 270.
[31] D. Ishimaru, L. R. Andrade, L. S. P. Teixeira, P. A. Quesado, L. M. Maiolino, P. M. Lopez, Y. Cordeiro, L. T. Costa, W. M. Heckl, G. Weissmüller, D. Foguel, J. L. Silva, *Biochemistry* **2003**, *42*, 9022.
[32] J. L. Silva, T. C. R. G. Vieira, M. P. B. Gomes, A. P. A. Bom, L. M. T. R. Lima, M. S. Freitas, D. Ishimaru, Y. Cordeiro, D. Foguel, *Acc. Chem. Res.* **2010**, *43*, 271 – 279.
[33] J. L. Silva, C. V. De Moura Gallo, D. C. F. Costa, L. P. Rangel, *Trends Biochem. Sci.* **2014**, *39*, 260 – 267.

[34] C. B. Levy, A. C. Stumbo, A. P. D. Ano Bom, E. A. Portari, Y. Cordeiro, Y. Carneiro, J. L. Silva, C. V. De Moura-Gallo, *Int. J. Biochem. Cell Biol.* **2011**, *43*, 60 – 64.
[35] J. Xu, J. Reumers, J. R. Couceiro, F. De Smet, R. Gallardo, S. Rudyak, A. Cornelis, J. Rozenski, A. Zwolinska, J.-C. Marine, D. Lambrechts, Y.-A. Suh, F. Rousseau, J. Schymkowitz, *Nat. Chem. Biol.* **2011**, *7*, 285.
[36] A. Soragni, D. M. Janzen, L. M. Johnson, A. G. Lindgren, A. Thai-Quynh Nguyen, E. Tiourin, A. B. Soriaga, J. Lu, L. Jiang, K. F. Faull, M. Pellegrini, S. Memarzadeh, D. S. Eisenberg, *Cancer Cell* **2016**, *29*, 90 – 103.
[37] S. Ghosh, D. Ghosh, S. Ranganathan, A. Anoop, P. S. Kumar P., N. N. Jha, R. Padinhateeri, S. K. Maji, *Biochemistry* **2014**, *53*, 5995 – 6010.
[38] A. P. D. Ano Bom, L. P. Rangel, D. C. F. Costa, G. A. P. de Oliveira, D. Sanches, C. A. Braga, L. M. Gava, C. H. I. Ramos, A. O. T. Cepeda, A. C. Stumbo, C. V. De Moura Gallo, Y. Cordeiro, J. L. Silva, *J. Biol. Chem.* **2012**, *287*, 28152 – 28162.
[39] P. A. J. Muller, K. H. Vousden, *Cancer Cell* **2014**, *25*, 304 – 317.
[40] J. W. K. Ng, D. Lama, S. Lukman, D. P. Lane, C. S. Verma, A. Y. L. Sim, *Proteins Struct. Funct. Bioinf.* **2015**, *83*, 2240 – 2250.
[41] W. Hanel, N. Marchenko, S. Xu, S. X. Yu, W. Weng, U. Moll, *Cell Death Differ.* **2013**, *20*, 898 – 909.
[42] D. Tempé, M. Brengues, P. Mayonove, H. Bensaad, C. Lacrouts, M. C. Morris, *Biochemistry* **2007**, *46*, 45 – 54.
[43] B. Dumat, G. Bordeau, A. I. Aranda, F. Mahuteau-Betzer, Y. El Harfouch, G. Metge, F. Charra, C. Fiorini-Debuisschert, M. P. Teulade-Fichou, *Org. Biomol. Chem.* **2012**, *10*, 6054 – 6061.
[44] M. Pellerano, *ChemBioChem* **2016**, *17*, 737 – 744.
[45] D. T. Yang, X. Lu, Y. Fan, R. M. J. Murphy, *AIChE J.* **2014**, *60*, 1236 – 1244.
[46] M. C. Morris, J. Depollier, J. Mery, F. Heitz, G. Divita, *Nat. Biotechnol.* **2001**, *19*, 1173 – 1176.

Manuscript received: September 7, 2018
Revised manuscript received: December 10, 2018
Accepted manuscript online: December 13, 2018
Version of record online: January 24, 2019